



# Role of the alumina surface properties on the ammonia production during the NO<sub>x</sub> SCR with ethanol over Ag/Al<sub>2</sub>O<sub>3</sub> catalysts

Fabien Can<sup>a,\*</sup>, Aurélien Flura<sup>a</sup>, Xavier Courtois<sup>a</sup>, Sébastien Royer<sup>a</sup>, Gilbert Blanchard<sup>b</sup>, Patrice Marécot<sup>a</sup>, Daniel Duprez<sup>a</sup>

<sup>a</sup> Université de Poitiers, Laboratoire de Catalyse en Chimie Organique, UMR 6503 CNRS, 40 Avenue du Recteur Pineau, 86022 Poitiers cedex, France

<sup>b</sup> Peugeot SA, Route de Gizey, 78943 Velizy-Villacoublay cedex, France

## ARTICLE INFO

### Article history:

Available online 4 November 2010

### Keywords:

Ag/Al<sub>2</sub>O<sub>3</sub>  
EtOH-SCR  
Ammonia  
NH<sub>3</sub> selectivity  
Alumina surface properties  
Infrared  
LAS

## ABSTRACT

The Selective Catalytic Reduction of NO<sub>x</sub> with ethanol (EtOH-SCR) was studied over Ag/Al<sub>2</sub>O<sub>3</sub> catalysts. A special attention was given to the ammonia emission and its possible relationship with the support acidic properties. For this purpose, five aluminas were selected, three provided by manufacturers and two synthesized in our laboratory by sol–gel or precipitation route. The supports were impregnated with 2 wt.% Ag, and tested in EtOH-SCR. The results showed that the catalytic activity of Ag/Al<sub>2</sub>O<sub>3</sub> greatly depends on the used alumina. An unexpected ammonia production is evidenced, varying between 6 and 27% at 450 °C, while NO<sub>x</sub> are fully converted. A correlation was established between the NH<sub>3</sub> yield and the Lewis acid sites (LAS) density measured by pyridine adsorption for each catalyst.

© 2010 Elsevier B.V. All rights reserved.

## 1. Introduction

In this current period where the reduction of carbon dioxide emission become more and more severe, the solution to use engine working in lean condition remains very attractive. However, in this condition (i.e., in excess of oxygen), the usual three-way catalyst is inefficient in NO<sub>x</sub> reduction. These last few years saw the emergence of two usual catalytic processes to reduce NO<sub>x</sub> from these engine exhausts. One possible solution is the use of the NO<sub>x</sub> storage reduction (NSR) catalyst [1], working in transient periods: during the lean condition, NO<sub>x</sub> are firstly oxidized and stored as nitrites or nitrates on a basic material, usually barium oxide. Periodically, the catalyst is regenerated: the stored NO<sub>x</sub> are reduced in N<sub>2</sub> during a short excursion in rich condition. Nevertheless the major drawback of this system is the deactivation of the catalyst, mainly due to sulfur poisoning [2,3], and the thermal aging [4,5]. The second way is the Selective Catalytic Reduction (SCR) of NO<sub>x</sub>. Numerous reducers have been investigated in the literature, such as hydrocarbons [6–13], oxygenated compounds [10,11,14,15] and nitrogen containing compounds (ammonia, urea, ...) [15–19]. Recently, the SCR of NO<sub>x</sub> by ethanol over alumina supported silver catalysts has been extensively studied in the literature [20–23], due to his promising efficiency. Thereafter, numerous academic studies, dealing with

the effect of silver loading and precursor, reaction mechanism, role of adsorbed species, and nature of active Ag species [24–27] have been published. Different routes have been explored to improve the reaction efficiency, especially in order to raise the catalytic activity at low temperature (i.e., below 300 °C) [28,29]. Nevertheless, although ammonia has been suggested as a possible intermediate in the NO<sub>x</sub> SCR by hydrocarbons [30,31], no one directly focus, even in the more quoted papers, on the amount of NH<sub>3</sub> given out.

The present work focuses on the influence of the alumina chemical surface properties toward the NH<sub>3</sub> emission during the SCR of NO<sub>x</sub> by ethanol with Ag/Al<sub>2</sub>O<sub>3</sub> catalysts. Catalysts were characterized using XRD, TEM and infrared spectroscopy.

## 2. Experimental part

### 2.1. Catalyst preparation

The Al(1) Al<sub>2</sub>O<sub>3</sub> was synthesized as follows: an aluminum precursor (aluminum sec-butoxide, 97%, provided by Alfa Aesar) was dissolved in 1-butanol at 65 °C and stirred until complete dissolution. The process was carried out in the presence of a surfactant agent ((1-Hexadecyl) trimethylammonium, 98%, provided by Alfa Aesar). The two solutions were then mixed and kept at 65 °C under stirring. A limited amount of water was thereafter introduced under vigorous stirring, in order to start the hydrolysis of the aluminum precursor. The molar composition of the mixture was (Al:surfactant:1-butanol:water) = (0.5:1:10:2). Stirring was contin-

\* Corresponding author. Tel.: +33 0549453997; fax: +33 0549453741.  
E-mail address: [fabien.can@univ-poitiers.fr](mailto:fabien.can@univ-poitiers.fr) (F. Can).

ued for 4 h at 65 °C until homogeneity was obtained. Then, the hydrothermal reaction was followed at 100 °C for 24 h under auto-genous pressure and static condition. The product was washed several times with 1-butanol, and dried sequentially at room temperature during 24 h. Then, the obtained gel was dried in oven at 80 °C during 24 h. Finally, the dried gel was heat-treated in air at a rate of 3 °C min<sup>-1</sup> up to 600 °C, and kept at this temperature for 4 h before cooling.

The A(2) alumina was synthesized using the following process: an aluminium precursor (Al(NO<sub>3</sub>)<sub>3</sub>, 98%, provided by Alfa Aesar) was dissolved in water and stirred. An amount of NaAl<sub>2</sub>O<sub>4</sub> (Riedel-de Haën) was added subsequently to start the hydrolysis, and stopped when the pH of the resulting mixture reached 8. The solution was kept under stirring for 3 h, and then placed in oven at 80 °C for 20 h. The product was washed twice with 250 mL of slightly warm water (40 °C), and placed in oven during 48 h at 110 °C. Finally, the dried product was heat-treated in air at a rate of 3 °C min<sup>-1</sup> up to 600 °C, and kept at this temperature for 4 h before cooling.

The A(3), A(4) and A(5) alumina were provided by commercial manufacturers.

## 2.2. Surface and textural analysis

Transmission electron microscopy (TEM) analyses were obtained with a Philips CM 120 microscope operating at 120 kV, equipped with an energy-dispersive X-ray detector (EDX).

Nitrogen adsorption isotherms were performed at -196 °C using a Tristar 3000 Micromeritics apparatus. Prior to the measurement, the samples were pretreated at 250 °C under vacuum for 5 h. The surface area is calculated using the BET method.

XRD patterns were recorded in a Siemens D5000 diffractometer, equipped with a Cu anode ( $\lambda = 0.15406$  nm). Diffractograms were recorded in the 15–75° range of 2 $\theta$ , with a step of 0.04° and a dwell time of 6 s. Crystalline phases were identified by comparison with the corresponding JCPDS files.

## 2.3. Chemical surface properties

The surface acidity was evaluated by IR spectroscopy of adsorbed pyridine. IR spectra were recorded in a Nexus Nicolet spectrometer equipped with DTGS detector (Deuterium TriGlyc-eride Sulfur) and KBr beam splitter. IR spectra were recorded with a resolution of 4 cm<sup>-1</sup> and 64 scans. The presented spectra were normalized to a disc of 10 mg cm<sup>-2</sup>. After activation at 450 °C under vacuum, pyridine was adsorbed (200 Pa at equilibrium) at room temperature and further desorbed until 450 °C (by temperature step of 50 °C). The  $\nu_{8a}$  spectral regions were deconvoluted using the peak resolve function of the Omnic software, in order to obtain the amount of strong (Al<sup>3+</sup><sub>IV</sub>) and weak (Al<sup>3+</sup><sub>VI</sub>) Lewis acid sites (LAS). The total amount of LAS is determined from the area of the  $\nu_{19b}$  band, using its molar coefficient ( $\epsilon_{\nu_{19b}} = 1.5$  cm<sup>2</sup> μmol<sup>-1</sup> [32]). Hydroxyl groups of alumina were characterized by the study of IR spectra in the 3900–3500 cm<sup>-1</sup> range.

## 2.4. Catalytic tests

Catalytic tests were performed in a quartz tubular micro-reactor under a flow composed of 400 ppm NO, 500 ppm CO, 167 ppm H<sub>2</sub>, 1200 ppm C<sub>2</sub>H<sub>5</sub>OH, 8% O<sub>2</sub>, 10% H<sub>2</sub>O, 10% CO<sub>2</sub> balanced in N<sub>2</sub>, simulating realistic exhaust conditions. Gas flows were controlled using mass-flow controllers (Brooks), except for H<sub>2</sub>O and C<sub>2</sub>H<sub>5</sub>OH which were introduced using thermostated saturators. The GHSV is fixed at 150,000 h<sup>-1</sup>. Both NO and NO<sub>x</sub> concentrations (NO + NO<sub>2</sub>) were measured by chemiluminescence (Monitor Europe ML9841AS); CO and N<sub>2</sub>O were detected by FTIR analyzers (COSMA Beryl 100). Prior

**Table 1**

Textural properties of alumina supports.

	S <sub>BET</sub> (m <sup>2</sup> g <sup>-1</sup> )	V <sub>p</sub> (cm <sup>3</sup> g <sup>-1</sup> )	D <sub>p</sub> (nm)
Ag/A(1)	263	1.13	9.6
Ag/A(2)	186	0.29	5.3
Ag/A(3)	164	0.84	12.8
Ag/A(4)	156	0.48	9.4
Ag/A(5)	138	0.45	9.0

to the analyzers, H<sub>2</sub>O was removed in a condenser at 0 °C. For each studied temperature (150 °C, 250 °C, 300 °C, 350 °C, 450 °C and 550 °C), the activity of the catalysts was followed until stabilization. After stabilization, the outlet water was condensed for 30 min through bubbling the gas mixture in a clean condenser filled with 10 mL of demineralised water (pH ≈ 5.5), and then analyzed by two HPLC (Thermo Finnigan) for NH<sub>4</sub><sup>+</sup> (Alltech Universal Cation, 7 μm, 4.6 mm × 100 mm) and NO<sub>2</sub><sup>-</sup> and NO<sub>3</sub><sup>-</sup> (Agilent Eclipse XDB-C18, 5 μm, 4.6 mm × 50 mm). NO<sub>2</sub><sup>-</sup> and NO<sub>3</sub><sup>-</sup> were added to the unconverted NO<sub>x</sub>. An example of the calculation of the NH<sub>4</sub><sup>+</sup> concentration (ppm) species are reported here:

$$n(\text{NH}_4^+ \text{ trapped in 30 min}) [\text{mole}]$$

$$= C(\text{NH}_4^+ \text{ in condensed solution}) \times V(\text{condensed solution})$$

$$V(\text{NH}_3 \text{ gas}) [L] = n(\text{NH}_4^+ \text{ trapped in 30 min}) \times V_m$$

$$Q(\text{NH}_3 \text{ gas}) [\text{mL/min}] = \frac{[V(\text{NH}_3 \text{ gas}) \times 10^3]}{t(\text{condensation}) [\text{min}]}$$

$$[\text{NH}_3 \text{ gas}] [\text{ppm}] = \frac{[Q(\text{NH}_3 \text{ gas}) \times 10^6]}{Q(\text{gas mixture}) [\text{mL/min}]}$$

Ethanol conversion was measured using a Gas Chromatograph (Varian 3400, Supelco HayeSep R, 60–80 mesh, 1/8 in. × 2000 mm) equipped with a FID detector. The N<sub>2</sub> selectivity is calculated assuming no other N-compounds than NO, NO<sub>2</sub>, N<sub>2</sub>O, NH<sub>3</sub>. In order to validate our results, all the outlet gas (C<sub>2</sub>H<sub>5</sub>OH, CH<sub>3</sub>CHO, CH<sub>3</sub>OH, CH<sub>2</sub>O, C<sub>2</sub>H<sub>4</sub>, CO, NO, NO<sub>2</sub>, NH<sub>3</sub>, N<sub>2</sub>O) are regularly checked with a multigas infrared detector (MKS 2030).

## 3. Results and discussion

### 3.1. Catalysts characterization

Supported silver catalysts are characterized by XRD, TEM and IR. Results of the catalysts textural and structural characterizations are summarized in Table 1. Surface area varies between 138 m<sup>2</sup> g<sup>-1</sup> for A(5) and 263 m<sup>2</sup> g<sup>-1</sup> for A(1) sample, prepared using a modified sol–gel procedure. Pore volume and pore diameter are also widely spread.

X-ray diffraction patterns are presented in Fig. 1. The analysis evidences the formation of γ-Al<sub>2</sub>O<sub>3</sub> phase (JCPDS file no. 00-050-0741) for all samples with no visible reflection assigned to Ag<sup>0</sup> or AgO. The metallic silver particles are characterized by transmission electron spectroscopy (TEM). Whatever the studied sample, TEM analysis (figure not shown) allows to detect silver particles dispersed among the alumina aggregates, sizing between 4 and 7 nm. Some larger particles (around 20–35 nm) are also detected, in a lesser extent, showing that alumina physical properties have a limited effect on the silver dispersion.

To summarize, the textural and structural characterizations only show that the surface area of various alumina supports differs from a material to the other. No differences were observed between their crystalline phase and their metallic dispersion measurements.

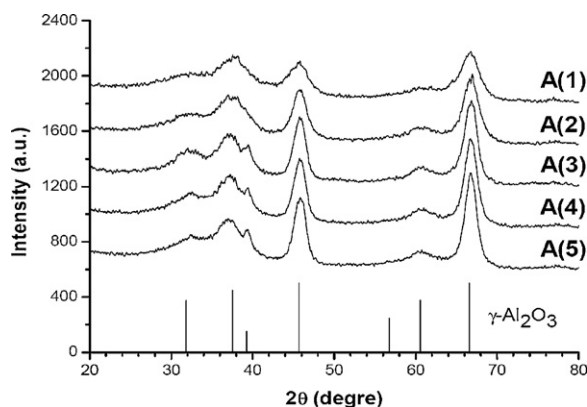


**Fig. 1.** XRD patterns of alumina supports.  $\gamma$ - $\text{Al}_2\text{O}_3$  structure [ICDD PDF no. 00-050-0741 (1)].

### 3.2. Catalytic test

Firstly, the reactivity of unsupported alumina A(1) support and the alumina silver supported (Ag/A(1)) catalyst was investigated. The ethanol conversion versus temperature was studied with or without  $\text{NO}_x$  in the gas mixture. Secondly, the conversion of  $\text{NO}_x$  in  $\text{N}_2$ , as well as the  $\text{NH}_3$  yield, was presented.

#### 3.2.1. Ethanol decomposition

The effect of  $\text{NO}_x$  in the ethanol conversion versus temperature is presented in Fig. 2 for A(1) support and Ag/A(1) catalyst. Firstly, the ethanol conversion is always higher on silver supported catalyst than on the support alone, with or without  $\text{NO}_x$  in the gas mixture. For instance, without  $\text{NO}_x$  (dotted line, Fig. 2), the ethanol conversion is about 40% at 250 °C for the Ag/A(1) catalyst whereas it reaches 18% for the A(1) corresponding support. Secondly, the ethanol conversion increases in the presence of  $\text{NO}_x$  in the gas mixture for both materials. Ethanol is totally converted at 350 °C for the alumina A(1) support as well as for the silver A(1) supported silver catalyst (Ag/A(1)).

Besides, it is well known in the literature that ethanol dehydrogenation and ethanol dehydration [33,34] are respectively catalyzed by basic (and metallic) or acidic sites. It results in the formation of acetaldehyde or ethylene, as mentioned in reactions (1) and (2):

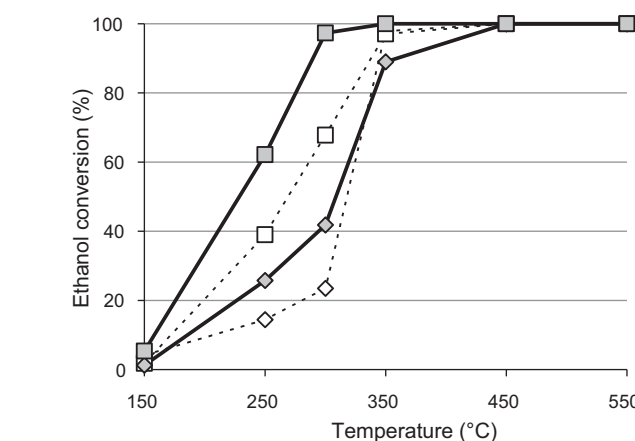
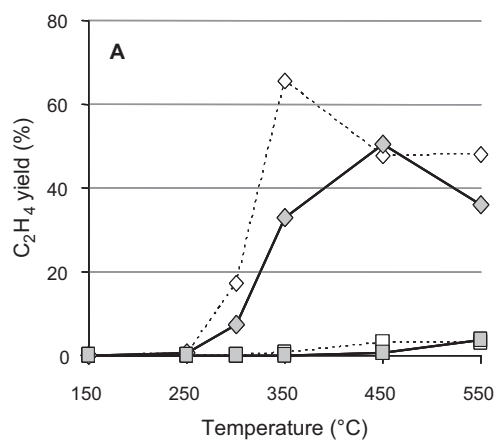
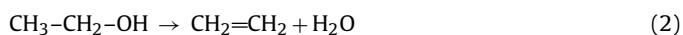
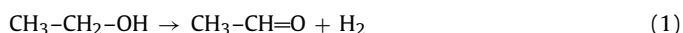


**Fig. 2.** Ethanol conversion in function of temperature for A(1) support ( $\diamond$ ) and Ag/A(1) catalyst ( $\square$ ). Blank symbols: without  $\text{NO}_x$ ; solid symbols: with  $\text{NO}_x$  in the gas mixture.

The  $\text{C}_2\text{H}_4$  and  $\text{CH}_3\text{CHO}$  yield are reported in Fig. 3 versus the temperature of catalytic test. For the alumina A(1) support, without  $\text{NO}_x$  in the gas mixture, the main product of the ethanol decomposition is ethylene, with a maximum yield of about 65% at 350 °C (dotted line, Fig. 3A). In presence of  $\text{NO}_x$ ,  $\text{C}_2\text{H}_4$  yield decreases, while  $\text{CH}_3\text{CHO}$  yield increases. Concerning the silver supported catalyst, different results are observed. The main ethanol decomposition compound is acetaldehyde, with a maximum yield shifted to the lower temperature, with about 30% at 250 °C. These results are in good agreement with the literature data which suggest that  $\text{C}_2\text{H}_4$  formation is catalyzed by acidic sites of the alumina support whereas the acetaldehyde production is rather catalyzed at low temperature by metallic sites.

#### 3.2.2. SCR of $\text{NO}_x$ by ethanol

Fig. 4 displays the  $\text{NO}_x$  conversion in  $\text{N}_2$  and the  $\text{NH}_3$  yield for the five silver supported materials. The  $\text{NO}_x$  conversion starts at 250 °C to become significant at 300 °C, and reaches a maximum from 350 °C to 450 °C. At this temperature, the catalytic behavior differs from a catalyst to the other. For instance, no significant amount of  $\text{N}_2\text{O}$  is measured, but the evolution of the ammonia yield versus the temperature, reported in Fig. 4B, clearly shows a high ammonia emission. Indeed, while reaction is selective into  $\text{N}_2$  at low temperature (below 300 °C, Fig. 4A), an increase in the  $\text{NH}_3$  yield is observed alongside the reaction temperature, the maximum being observed at 450 °C. Thus,  $\text{NH}_3$  yield varies as follow: Ag/A(1) > Ag/A(3) > Ag/A(2) > Ag/A(4) > Ag/A(5).

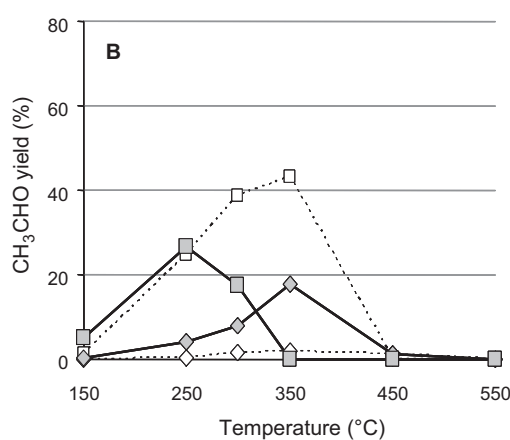


**Fig. 3.**  $\text{C}_2\text{H}_4$  (A) and  $\text{CH}_3\text{CHO}$  (B) yields versus temperature for A(1) support ( $\diamond$ ) and Ag/A(1) catalyst ( $\square$ ). In dotted line, catalytic results obtained without  $\text{NO}_x$  in the gas mixture.

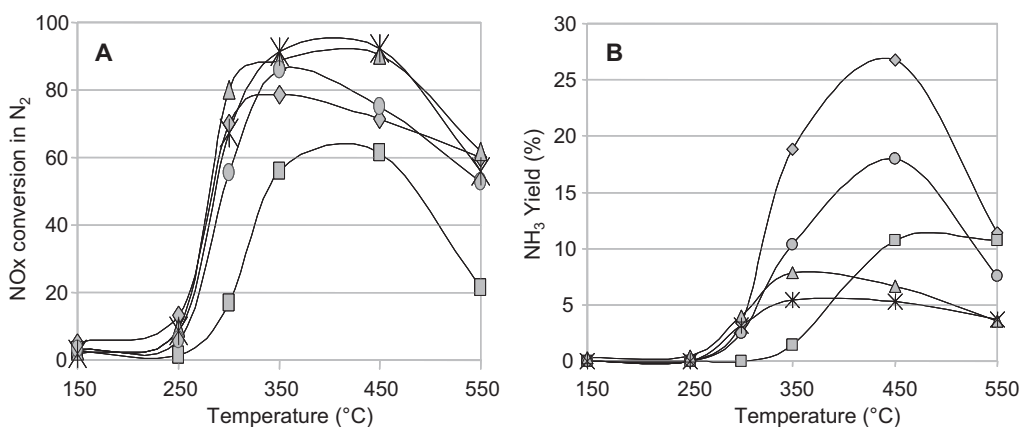


Fig. 4. NO<sub>x</sub> conversion in N<sub>2</sub> (A) and NH<sub>3</sub> yield (B) versus the alumina support and the catalytic temperature test.

NH<sub>3</sub> production is spread from a few percents for Ag/A(4) and Ag/A(5) to 27% for Ag/A(1). Such emission is, to our knowledge, not highlighted in the literature. One can note here that no ammonia formation is observed on silver free aluminas.

It has been shown previously that the textural properties of the five various alumina supports are very close. Thus, the high ammonia yields observed in Fig. 4B must be explained by other component, such as chemical surface properties. In this way, hydroxyl groups of alumina supports as well as acidic properties of catalysts have been characterized using pyridine adsorption monitored by infrared spectroscopy.

### 3.3. IR study

In Fig. 5, the IR spectra in the OH stretching region of silver supported on alumina catalysts were compared after outgassing at 450 °C. IR spectra are consistent with that reported in the literature [35], showing the different types of OH groups over alumina that display bands at 3790, 3773, 3726, 3686 and 3668 cm<sup>-1</sup>. Assignments are reported in Table 2. However one can note that the intensity of the band at 3726 cm<sup>-1</sup>, attributed to bridging hydroxyl (Al<sub>IV</sub>Al<sub>VI</sub>)OH type II, is significantly higher in the Ag/A(3) catalyst. In a same extent, the basic hydroxyl group characterized by the stretching OH frequency at 3773 cm<sup>-1</sup> is less dominant in this Ag/A(3) sample compared with the other supported silver catalysts.

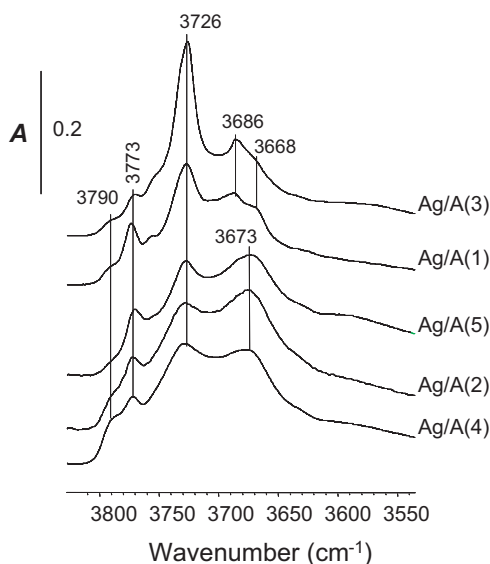
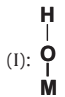
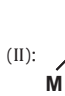
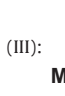


Fig. 5. IR spectra in the ν(OH) region of catalysts activated by outgassing at 450 °C.

Table 2

OH assignment on the surface of aluminas.

ν(OH) frequency (cm <sup>-1</sup> )	Type of OH group	Structure
3800–3785 3780–3760	(I): 	(Al <sub>VI</sub> )OH (Al <sub>IV</sub> )OH
3745–3740 3735–3730	(II): 	(Al <sub>VI</sub> ) <sub>2</sub> OH (Al <sub>IV</sub> Al <sub>VI</sub> )OH
3710–3700	(III): 	(Al <sub>VI</sub> ) <sub>3</sub> OH

The surface acidity was evaluated by IR spectroscopy of adsorbed pyridine, which is one of the most largely used basic probe molecules for surface acidity characterization [36,37]. After activation at 450 °C, pyridine was adsorbed (200 Pa at equilibrium) at room temperature and further desorbed at 300 °C (by temperature step of 50 °C), in order to eliminate physisorbed and H-bonded pyridine from the surface. IR spectra of the silver supported on various aluminas are presented in Fig. 6. Acidity is monitored by the ring vibration modes ν8a, ν8b, ν19a and ν19b of adsorbed pyridine, as studied by Parry [36]. IR adsorption band are then observed at 1624, 1618, 1577, 1495 and 1455 cm<sup>-1</sup>, assigned to coordinated pyri-

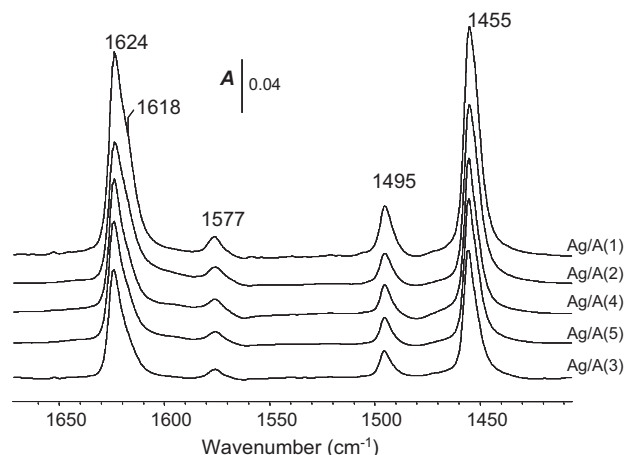
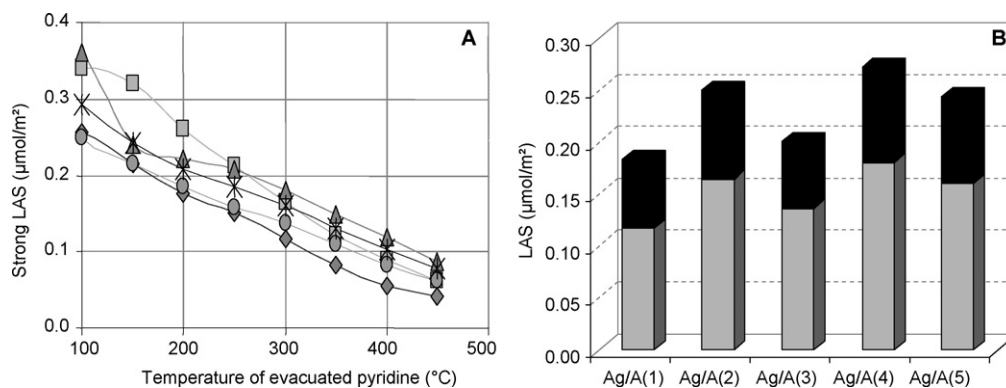
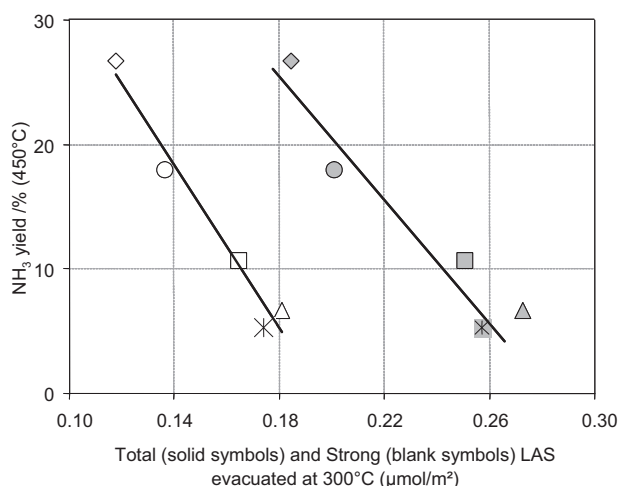


Fig. 6. IR difference spectra of pyridine desorbed at 300 °C.





**Fig. 7.** (A) Evolution of strong LAS density ( $\mu\text{mol}/\text{m}^2$ ) versus temperature of evacuated pyridine. ( $\blacklozenge$ ) Ag/A(1); ( $\square$ ) Ag/A(2); ( $\bullet$ ) Ag/A(3); ( $\triangle$ ) Ag/A(4); ( $\times$ ) Ag/A(5). (B) LAS density ( $\mu\text{mol}/\text{m}^2$ ) of coordinated pyridine desorbed at 300  $^{\circ}\text{C}$  evaluated after IR decomposition of  $\nu_{8a}$ . ( $\blacksquare$ ) Weak LAS; ( $\blacksquare$ ) strong LAS.

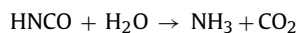


**Fig. 8.**  $\text{NH}_3$  yield at 450  $^{\circ}\text{C}$  versus the strong Lewis acid sites (LAS), evaluated from the  $\nu_{19b}$  and the  $\nu_{8a}$  IR band of the pyridine coordinated at 300  $^{\circ}\text{C}$ , in  $\mu\text{mol}/\text{m}^2$ . ( $\diamond$ ) Ag/A(1); ( $\square$ ) Ag/A(2); ( $\circ$ ) Ag/A(3); ( $\triangle$ ) Ag/A(4); ( $\times$ ) Ag/A(5).

dine on Lewis acid sites (LAS). No IR band assigned to pyridinium was observed, as expected on alumina which does not present OH groups strong enough to protonate the pyridine.

In the  $\nu_{8a}$  spectral range, two bands can be distinguished on these catalysts at 1624 and 1618  $\text{cm}^{-1}$ , assigned to pyridine respectively coordinated to tetrahedral  $\text{Al}^{3+}$  (strong LAS) and to both tetrahedral and octahedral  $\text{Al}^{3+}$  (medium LAS) coordinatively unsaturated sites (CUS). The deconvolution of the peaks occurring in the  $\nu_{8a}$  vibration range (figure not shown), may be used to describe the heterogeneous Lewis acidic character of studied catalysts in order to obtain the distribution of coordinated pyridine on each type of LAS. For instance, Fig. 7A exhibits the evolution of the density of strong ( $\nu_{8a}$  at 1624  $\text{cm}^{-1}$ ) LAS versus the temperature of evacuated pyridine. Firstly, comparison between aluminas support and silver supported catalysts show that metallic particles have no effect on the infrared spectra. In Fig. 7B is shown the distribution between weak and strong LAS, determinates from pyridine coordinated on alumina CUS at 300  $^{\circ}\text{C}$ . Several points should be noted. First, Fig. 7B informs that alumina support do not display the same density of LAS. The Ag/A(4) catalyst exhibits the higher amount of LAS, whereas Ag/A(1) presents the lesser LAS density. Secondly, the distribution between strong and weak LAS varies greatly, inferring a strong Lewis acid sites ranged from 0.12  $\mu\text{mol}/\text{m}^2$  to 0.18  $\mu\text{mol}/\text{m}^2$ , which leads to the following order: Ag/A(4) > Ag/A(5) > Ag/A(2) > Ag/A(3) > Ag/A(1).

In the literature [38], the hydrolysis reaction of HNCO has been forwarded for the ammonia production, via the following reaction:



Recently [39], a real-time infrared experiment showed that strong ( $\text{Al}^{3+}_{\text{IV}}$ ) and weak ( $\text{Al}^{3+}_{\text{VI}}$ ) Lewis acid sites were involved in the  $-\text{NCO}$  spill over, through a transfer of the isocyanate from  $\text{Al}_{\text{VI}}$  to  $\text{Al}_{\text{IV}}$ . Since isocyanate species are generally assumed as a precursor to ammonia, the amount of  $\text{NH}_3$  yield was regarded as a function of the strong Lewis acid site density. Indeed, Fig. 8 illustrates the correlation between the  $\text{NH}_3$  yield and the amount of strong or total LAS density, evaluated from pyridine coordinated at 300  $^{\circ}\text{C}$ . Similar results can be obtained while using the  $\text{Al}^{3+}_{\text{IV}}/\text{Al}^{3+}_{\text{VI}}$  ratio. In fact, the  $\text{Al}^{3+}_{\text{IV}}/\text{Al}^{3+}_{\text{VI}}$  ratio is independent from the catalysts surface area and can also be used to assess the strong to weak LAS balance. It was assumed that the higher the density of strong LAS, the lower the  $\text{NH}_3$  emission. This correlation clearly evidences the role of acidic properties of alumina support on the mechanism of ammonia production for  $\text{NO}_x$  SCR with ethanol.

#### 4. Conclusion

In this work, the Selective Catalytic Reduction of  $\text{NO}_x$  by ethanol over alumina supported silver catalyst was studied. Five alumina supports were investigated. Firstly, catalyst characterizations show that alumina physical and textural properties have a limited effect on the metallic silver particles size. However it was demonstrated that hydroxyl groups and Lewis acid sites distribution differ versus the aluminum oxide. Catalytic tests show that Ag/ $\text{Al}_2\text{O}_3$  obviously presents high activity for the SCR of  $\text{NO}_x$  with ethanol, as extensively reported in the literature. Surprisingly, a high and unexpected ammonia emission was also reported here (up to 27%). A correlation between the  $\text{NH}_3$  yield and the acidic surface properties of the alumina support was likewise reported.

This study evidenced the importance of the support surface acid–base properties, which need to be controlled in order to maintain ammonia production in reaction at an acceptable level.

#### References

- [1] W.S. Epling, L.E. Campbell, A. Yezzerets, N.W. Currier, J.E. Parks II, Catal. Rev. 46 (2004) 163.
- [2] C. Sedlmair, K. Seshan, A. Jentys, J.A. Lercher, Catal. Today 75 (2002) 413.
- [3] E.C. Corbos, X. Courtois, N. Bion, P. Marecot, D. Duprez, Appl. Catal. B 80 (2008) 62.
- [4] D. Uy, A.E. O'Neill, J. Li, W.L.H. Watkins, Top. Catal. 95 (2004) 191.
- [5] M. Casapu, J.D. Grunwaldt, M. Maciejewski, M. Wittrock, U. Göbel, A. Baiker, Appl. Catal. B 63 (2006) 232.
- [6] M. Konsolakis, I.V. Yentekakis, J. Catal. 198 (2001) 142.

- [7] J. Shibata, K.-I. Shimizu, A. Satsuma, T. Hattori, *Appl. Catal. B* 37 (2002) 197.
- [8] E.F. Iliopoulou, A.P. Evdou, A.A. Lemonidou, I.A. Vasalos, *Appl. Catal. A* 274 (2004) 179.
- [9] L.F. Cordoba, W.M.H. Sachtler, C.M. de Correa, *Appl. Catal. B* 56 (2005) 269.
- [10] T. Maunula, J. Ahola, H. Hamada, *Appl. Catal. B* 26 (2000) 173.
- [11] E. Joubert, X. Courtois, P. Marecot, D. Duprez, *Appl. Catal. B* 64 (2006) 103.
- [12] P. Denton, A. Giroir-Fendler, H. Praliaud, M. Primet, *J. Catal.* 189 (2000) 410.
- [13] F. Figueras, J.L. Flores, G. Delahay, A. Giroir-Fendler, A. Bouranea, J.-M. Clacens, A. Desmartin-Chomel, C. Lehaut-Burnouf, *J. Catal.* 232 (2005) 27.
- [14] D. Tran, C.L. Aardahl, K.G. Rappe, P.W. Park, C.L. Boyer, *Appl. Catal. B* 48 (2004) 155.
- [15] K.O. Haj, S. Ziyade, M. Ziyad, F. Garin, *Appl. Catal. B* 37 (2002) 49.
- [16] N.W. Cant, A.D. Cowan, I.O.Y. Liu, A. Satsuma, *Catal. Today* 5 (1999) 473.
- [17] N.W. Cant, I.O.Y. Liu, *Catal. Today* 63 (2000) 133.
- [18] V. Zuzaniuk, F.C. Meunier, J.R.H. Ross, *J. Catal.* 202 (2001) 340.
- [19] I.O.Y. Liu, N.W. Cant, *J. Catal.* 230 (2005) 123.
- [20] N. Bion, J. Saussey, M. Haneda, M. Daturi, *J. Catal.* 217 (2003) 47.
- [21] Y.H. Yeom, M. Li, W.M.H. Sachtler, E. Weitz, *J. Catal.* 246 (2007) 413.
- [22] H. He, Y. Yu, *Catal. Today* 100 (2005) 37.
- [23] A. Obuchi, I. Kaneko, J. Oi, A. Ohi, A. Ogata, G.R. Bamwenda, S. Kushiya, *Appl. Catal. B* 15 (1998) 37.
- [24] K. Shimizu, A. Satsuma, *Phys. Chem. Chem. Phys.* 6 (2006) 2677.
- [25] X. Zhang, H. He, Z. Ma, *Catal. Commun.* 8 (2007) 187.
- [26] Y. Yu, H. He, Q. Feng, *J. Phys. Chem. B* 107 (2003) 13090.
- [27] Y. Yeom, M. Li, A. Savara, W. Sachtler, E. Weitz, *Catal. Today* 136 (2008) 55.
- [28] K. Sato, T. Yoshinari, Y. Kintaichi, M. Haneda, H. Hamada, *Appl. Catal. B* 44 (2003) 67.
- [29] H. He, J. Wang, Q. Feng, Y. Yu, K. Yoshida, *Appl. Catal. B* 46 (2003) 365.
- [30] F. Poignant, J. Saussey, J.-C. Lavalley, G. Mabilon, *J. Chem. Soc., Chem. Commun.* (1995) 89.
- [31] F. Poignant, J.L. Freysz, M. Daturi, J. Saussey, *Catal. Today* 70 (2001) 197.
- [32] S. Khabtou, T. Chevreau, J.C. Lavalley, *Micropor. Mater.* 3 (1994) 133.
- [33] F. Can, A. Le Valant, N. Bion, F. Epron, D. Duprez, *J. Phys. Chem. C* 112 (2008) 14145.
- [34] A. Le Valant, N. Bion, F. Can, D. Duprez, F. Epron, *Appl. Catal. B* 97 (2010) 72.
- [35] H. Knözinger, P. Ratnasamy, *Catal. Rev.—Sci. Eng.* 17 (1978) 31.
- [36] E.P. Parry, *J. Catal.* 2 (1963) 371.
- [37] H. Knözinger, *Adv. Catal.* 25 (1976) 184.
- [38] N. Macleod, R.M. Lambert, *Chem. Commun.* 9 (2003) 1300.
- [39] F. Thibault-Starzyk, E. Seguin, S. Thomas, M. Daturi, H. Arnolds, D.A. King, *Science* 324 (2009) 1048.